İSTANBUL UNIVERSITY CERRAHPAŞA

RESEARCH ARTICLE

Electrica, 2021; 21(1): 105-114

Secrecy Capacity Analysis of an Underlay Cognitive Radio Network in the Presence of Co-channel and Primary Network Interference

Emre Bayat, Sultan Aldırmaz Çolak

Department of Electronics and Communication Engineering, Kocaeli University, Kocaeli, Turkey

Cite this article as: Bayat E, Aldırmaz Çolak S. Secrecy Capacity Analysis of an Underlay Cognitive Radio Network in the Presence of Co-channel and Primary Network Interference. *Electrica*, 2021; 21(1): 105-114.

ABSTRACT

This study investigates the impact of primary network and co-channel interference on the secrecy outage probability and strictly positive secrecy capacity of an underlay cognitive decode-and-forward relay network in Rayleigh fading channels. We consider a single eavesdropper node that tries to steal the transmitted signal at each hop. The secrecy outage probability and the strictly positive secrecy capacity are theoretically derived as a function of the interference sources and fading channels, which has not been studied in the literature. The theoretical results are validated with Monte Carlo simulation results. Consequently, the results show that the secrecy outage probability and the strictly positive secrecy capacity drastically degrade when the number of co-channel interference sources and the PN interference power increase.

Keywords: Underlay cognitive radio, secrecy outage probability, co-channel interference, decode-and-forward, cooperative communication

Corresponding Author:
Emre Bayat

E-mail:
emrebayat@gmail.com

Received: 19.05.2020

Accepted: 17.10.2020

DOI: 10.5152/electrica.2021.20054

Introduction

With the introduction of fifth-generation communication into our lives, millions of devices are estimated to be added to the existing network with diverse applications in a very wide band from 700 MHz to 100 GHz [1]. Efficient resource allocation techniques will be one of the most crucial functions due to the frequency spectrum scarcity. Network densification was popularized years ago to exploit the frequency resources more efficiently and increase the number of users served. High spectrum utilization is caused by the aggressive employment of reuse strategies of the same frequency channels, which results to a co-channel interference (CCI).

The cognitive radio (CR) network proposed by Mitola in [2] can be considered as another solution to a more efficient usage of the frequency spectrum. In CR, three main spectrum access techniques enable unlicensed users, which are also known as secondary users (SUs), to access the licensed bands of primary users (PUs), namely underlay, overlay, and interweave [3]. This classification is roughly made by specifying under which conditions SUs can access the system. In underlay and overlay systems, SUs can simultaneously access the system with PUs. In an interweave system, SUs can only access the system when PUs do not exist in the frequency band.

The underlay approach is more popular than other spectrum access techniques in CR networks (CRNs) [4-12]. The key point of an underlay CRN (UCRN) is that the SU's transmission power, which causes interference on the PUs, is limited by a predefined interference level to ensure the desired quality of service (QoS) of PUs. In [4, 5], the outage performance of a cooperative CRN that employs a decode-and-forward (DF) relaying protocol was investigated. In [6-12], performance was analyzed for a dual-hop CRN, where no direct communication exists between the source and destination nodes in the secondary network (SN). Multi relays were employed in the SN investigated in [7, 8]. Consequently, the system performance was found to be improved by using multiple secondary relays.

The system performance is affected by the CCI because CR networks are based on the co-existence of licensed and unlicensed users. It may be caused by adjacent sources using the same

frequency in other networks or in other unlicensed users in the CRN [9]. The impact of the CCI on the CRN performance is widely studied in the literature [9-12]. For example, in [9], the performance of opportunistic scheduling in DF-CRN in the presence of the CCI was investigated in terms of the outage probability, average error probability, and ergodic capacity. Aside from the CCI, the primary network (PN) causes interference on the SN because PUs and SUs can exist in the UCRN at the same time. The PN interference was also considered in [10] and [11] to investigate the outage performance of the UCRN over Rayleigh and Nakagami-m fading channels, respectively. These studies showed that both CCI and PN interferences severely degrade the system's outage performance. Another study [12] investigated the multi-hop outage performance with various antenna selection methods, showing that employing the multi-hop relay scheme in SN for UCRN enhances the system performance by reducing the effect of the interference power constraint.

The transmitted data can be stolen by illegal users due to the nature of wireless communication systems. To prevent illegal eavesdropping, information security can be ensured by data encryption–decryption algorithms developed at the application layer. However, these algorithms require high computational power, complex architecture, and high implementation cost. The physical layer security (PLS) emerged as an alternative to encryption applications because it has advantages, such as low computational complexity and low power consumption. Unlike encryption approaches, PLS secures privacy by using the time-varying properties of wireless channels, such as fading and noise [13, 14]. More specifically, the basic idea of the PLS is to evaluate whether the achievable rate of the legal transmission channel is higher than that of the wiretap channel (i.e., channel between the source and the eavesdropper).

The PLS investigation in the CRN has attracted the attention of many researchers [15-22]. In [15, 16], the PLS was extensively examined along with various attack scenarios. The secrecy outage probability (SOP) for multiple-input single-output and single-input multiple-output CRN was investigated in [17, 18]. The PLS in the dual-hop UCRN was discussed in [19, 20]. Lei et al. compared the secrecy performances of the dual-hop UCRN over Nakagami-m fading channels by using different relay selection techniques [19]. Meanwhile, [20] showed that SOP worsens as the number of PUs increases. In [21], closed-form expressions of the probability of the strictly positive secrecy capacity (SPSC) and the SOP were derived over generalized Gamma fading channels for a single-input single-output system.

This study presents the importance of considering the impact of the PN interference on the secrecy performance. Yang et al. [22] analyzed the effect of the CCI on the SOP performance. In [9], the outage probability and the bit error rate were investigated for the same system model. However, no analytical and simulation results for the SOP and the SPSC were obtained. Similarly, [22] only performed an SOP analysis. Both [9] and [22] investigated only the CCI effect on the other secondary sources. Inspired by this observation, we merged these two studies and performed SOP and SPSC analyses of a dual-hop UCRN considering the CCI from other SUs and the PN interference.

The contributions of this study are as follows:

- To make the analysis of [22] more realistic, we used the UCRN system model defined in [11], where the PN interference power is considered in the SN performance.
- In addition to the SOP analysis, unlike [22], we also performed an SPSC analysis under the CCI of the SN and the interference from the PN.
- Analytical expressions for the SOP and the SPSC were derived using MATHEMATICA. Their results were validated with Monte Carlo simulation results using MATLAB.

The remainder of this paper is organized as follows: Section 2 describes the UCRN system model; Section 3 presents the theoretical analyses for the SOP and the SPSC; Section 4 discusses the simulation results; and finally, Section 5 concludes the paper.

Notation: We use the following notation throughout the paper: probability operator: Pr (.); and cumulative distribution function (CDF) and probability density function (PDF): F (.) and f (.), respectively. Table 1 summarizes the system parameters used.

System Model

Figure 1 presents the proposed system model for the UCRN. This system model is originally defined in [11]. We only added an eavesdropper node to the SN. In the figure, S, R, and D represent the source, relay, and destination nodes in the SN, respectively. Moreover, E denotes an eavesdropper in the SN that attempts to steal information between S–E the and R–E nodes.

Table 1. Definition of parameters and symbols

Parameter	Definition
$h_i\ i \in \{sr,rd,sp,rp,pr,pd,ir,id\}$	Rayleigh channel coefficient
$\lvert h_j \rvert^2\ j \in \{sr,rd,sp,rp,pr,pd,ir,id\}$	Rayleigh channel gain
$\sigma_k^2\ k \in \{sr,rd,sp,rp,pr,pd,ir,id\}$	Rayleigh channel variance
C_s	Achievable rate of channel
$C_i^{eq}\ i \in \{sr,rd,e2e\}$	Secrecy achievable rate
$\gamma_i^{eq}\ i \in \{sr,rd,re,se\}$	SINR
P_{max}	Maximum allowable transmit power
I_{max}	Maximum interference threshold
γ_{th}	Secrecy threshold
$L_{R,D}$	Number of CCI sources

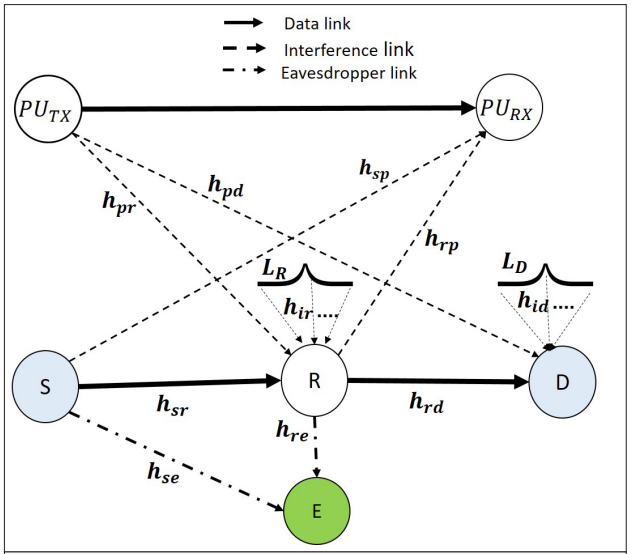

Figure 1. UCRN System Model with CCI and Primary Network Interference.

PU_{TX} and PU_{RX} represent the PN transmitter and receiver, respectively. Each node is equipped with a single antenna. We assume that no direct link exists between nodes S and D; thus, relay-assisted communication is employed in the SN, where the relay uses the DF scheme. The secondary transmission is simultaneously realized with the primary transmission; thus, its maximum transmit power is limited by I_{max}. In this manner, the QoS of the PN transmission is guaranteed.

All channels between nodes are assumed to be experienced as independent and non-identical (i.n.i.d) Rayleigh fading. The interference powers of the CCI sources are considered the same; thus, the CCI fading channels are assumed independent and identical (i.i.d) [9]. The channel fading coefficients between the S–R and R–D links are represented as h_{sr} and h_{rd}, respectively. h_{re} and denote the wiretap channel fading coefficients between the S–E and R–E links, respectively. While h_{pr} and h_{pd} represent the PN interference to nodes R and D, respectively, in the SN, h_{sp} and h_{rp} represent the interference channel coefficients from the SN to the PN, respectively. The channel coefficients from the CCI sources to the R and D links are represented as h_{ir} and h_{id}, respectively. The number of CCI sources at the R and D nodes is represented as L_R and L_D, respectively. The fading channels are assumed to be Rayleigh distributed; therefore, the channel gains follow $|h_{sr}|^2$, $|h_{rd}|^2$, $|h_{sp}|^2$, $|h_{rp}|^2$, $|h_{ir}|^2$, $|h_{id}|^2$, $|h_{pr}|^2$, and $|h_{pd}|^2$, with variances of σ_{sr}^2, σ_{rd}^2, σ_{sp}^2, σ_{rp}^2, σ_{pr}^2, σ_{pd}^2, σ_{ir}^2, and σ_{id}^2, respectively.

The SN transmission is performed in two steps considering the usage of relay-assisted communication. In the first step, the data are transmitted from node S to node R. Aside from the desired signals from node S, node R also receives undesired signals, such as an additive white Gaussian noise (AWGN) and an interference due to the CCI from the L_R interference sources, and PN. In the second step, node D receives the forwarded signal from node R together with the noise and interference signals similar to the first step. At the same time, the eavesdropper is active and tries to steal the transmitted signal from both the S and R nodes. The received signals at the R and S nodes are written as follows:

$$y_r = \sqrt{E_S}h_{sr}x + \sqrt{E_{IR}}\sum_{j=1}^{L_R} h_{ir_j}x_{r_j} + \sqrt{E_{PR}}h_{pr}x_{pr} + n_r \ , \tag{1}$$

$$y_d = \sqrt{E_R}h_{rd}\hat{x} + \sqrt{E_{ID}}\sum_{l=1}^{L_D} h_{id_l}x_{d_l} + \sqrt{E_{PD}}h_{pd}x_{pd} + n_d \ , \tag{2}$$

where E_S, and E_R are the transmit powers of the S and R nodes, respectively. Their values are determined by $E_S = \min\left(P_{max}, \frac{I_{max}}{|h_{sp}|^2}\right)$ and $E_R = \min\left(P_{max}, \frac{I_{max}}{|h_{rp}|^2}\right)$, where P_{max} is the maximum transmission power limit at both the S and R nodes. E_{IR} and E_{ID} are the energies of the CCI at nodes R and D, respectively. Furthermore, E_{PR} and E_{PD} represent the energy of the PN interference signals at nodes R and D, respectively. As in [11, 22], we assumed that all the CCIs have an equal power to simplify the analysis. In (1) and (2), n_r and n_d represent the AWGN with variance N_0.

The signal-to-interference plus noise ratio (SINR) of the S–R and R–D links is written as

$$\gamma_{sr}^{eq} = \frac{\frac{E_S}{N_0}|h_{sr}|^2}{1 + \frac{E_{IR}}{N_0}\sum_{j=1}^{L_R}\left|h_{ir_j}\right|^2 + \frac{E_{PR}}{N_0}\left|h_{pr}\right|^2} \ , \tag{3}$$

$$\gamma_{rd}^{eq} = \frac{\frac{E_R}{N_0}|h_{rd}|^2}{1 + \frac{E_{ID}}{N_0}\sum_{l=1}^{L_D}\left|h_{id_l}\right|^2 + \frac{E_{PD}}{N_0}\left|h_{pd}\right|^2} \ . \tag{4}$$

Moreover, the SINR of the eavesdropper links between S–E and R–E can be written as

$$\gamma_K^{eq} = \frac{E_T}{N_0}|h_K|^2, \tag{5}$$

where, $T \in \{S, R\}$ and $\in \{se, re\}$. The achievable rate $c_i \ i \in \{sr, se, rd, re\}$ of all links can be easily obtained as stated in [23]:

$$C_s = \log_2\left(1 + \gamma_s^{eq}\right). \tag{6}$$

The secrecy achievable rate is defined as the difference of the achievable rate of the channels between a legal user and an eavesdropper. Thus, the secrecy achievable rate expression per hop is written as in Eqs. (7) and (8).

$$C_{sr}^{eq} = \left(\log_2\left(1 + \gamma_{sr}^{eq}\right) - \log_2\left(1 + \gamma_{se}^{eq}\right)\right) = \log_2\left(\frac{1 + \gamma_{sr}^{eq}}{1 + \gamma_{se}^{eq}}\right), \tag{7}$$

$$C_{rd}^{eq} = \left(\log_2\left(1+\gamma_{rd}^{eq}\right) - \log_2\left(1+\gamma_{re}^{eq}\right)\right) = \log_2\left(\frac{1+\gamma_{rd}^{eq}}{1+\gamma_{re}^{eq}}\right). \quad (8)$$

The UCRN system uses the DF scheme; thus, the end-to-end secrecy achievable rate C_{e2e}^{eq} depends on the minimum achievable rate of the S–R and R–D links and can be written as follows:

$$C_{e2e}^{eq} = \log_2\left(\min\left(C_{sr}^{eq}, C_{rd}^{eq}\right)\right). \quad (9)$$

Secrecy Analysis

Secrecy Outage Probability

The SOP is the key performance metric for evaluating the security of communication systems. A secrecy outage occurs if C_{e2e} falls below a predefined secrecy rate ($R_s = \log_2(y_{th})$). The general expression of the CDF of the SOP is given as

$$F_{\gamma_{sr}} = \Pr(C_{e2e} \le R_s), \quad (10)$$

The SOP can be expressed as follows by using Eq. (9):

$$F_{\gamma_{sr}} = \Pr\left(\min\left(\underbrace{\frac{1+\gamma_{sr}^{eq}}{1+\gamma_{se}^{eq}}}_{C_{sr}^{eq}}, \underbrace{\frac{1+\gamma_{rd}^{eq}}{1+\gamma_{re}^{eq}}}_{C_{rd}^{eq}}\right) \le \gamma_{th}\right), \quad (11)$$

$$F_{\gamma_{sr}} = 1 - \left[1 - F_{\gamma_{sr}}(\gamma_{th})\right]\left[1 - F_{\gamma_{rd}}(\gamma_{th})\right], \quad (12)$$

where, $y_{th} = 2^{R_S}$, and $F_{y_{sr}}(y_{th})$, and $F_{y_{rd}}(y_{th})$ represent the SOP of the first and second hops, respectively.

According to the maximum interference and the power constraints on the CDF of the first hop, $F_{y_{sr}}(y_{th})$ can be expanded and expressed as

$$F_{\gamma_{sr}}(\gamma_{th}) = \overbrace{\Pr\left(\frac{1+\frac{I_{max}}{|h_{sp}|^2}|h_{sr}|^2}{1+\frac{\sum_{j=1}^{L_R}\left|h_{ir_j}\right|^2+|h_{pr}|^2+1}{1+\frac{I_{max}}{|h_{sp}|^2}|h_{se}|^2}} \le \gamma_{th}, \frac{I_{max}}{|h_{sp}|^2} < P_{max}\right)}^{P_1}$$
$$+ \overbrace{\Pr\left(\frac{1+\frac{P_{max}|h_{sr}|^2}{\sum_{l=1}^{L_R} IR_l + I_{PR}+1}}{1+P_{max}|h_{se}|^2} \le \gamma_{th}\right)}^{P_2} \times \overbrace{\Pr\left(\frac{I_{max}}{|h_{sp}|^2} > P_{max}\right)}^{P_3}. \quad (13)$$

As stated in [22], the P_1 term can be written as

$$P_1 = \int_{\frac{I_{max}}{P_{max}}}^{\infty} F_X(z) f_{h_{sp}}(z) dz. \quad (14)$$

Proposition 1: P_1 can be obtained as

$$\begin{aligned} P1 &= \exp\left(-\frac{I_{max}}{\sigma_{sp}^2 P_{max}}\right) \\ &+ \left(\frac{1}{a_1\sigma_{sp}^2 L_R!}\right)(T_1(-1)^{L_R})\exp\left(-\frac{I_{max}\left(\frac{1}{\sigma_{sp}^2}-T_2\right)}{P_{max}}\right) \\ &\times\left(Ei(-c1) - \exp\left(\frac{a_1c_1}{b_1}\right)Ei\left(-c_1-\frac{a_1c_1}{b_1}\right)\right) \\ &+ \sum_{n=0}^{L_R-1}\frac{T_1(-1)^{L_R}}{T_3T_4\sigma_{sp}^2L_R}(-1)^n n!\left(\frac{1}{T_3T_4\sigma_{sp}^2}-\frac{T_2}{T_3T_4}+1\right)^n \\ &\times\exp\left(\frac{\left(\frac{1}{\sigma_{sp}^2}-T_2\right)\sigma_{sr}^2 I_{max}}{T_4}\right) \\ &\times\Gamma\left(-n,\left(\frac{1}{T_3T_4\sigma_{sp}^2}-\frac{T_2}{T_3T_4}+1\right)\left(\sigma_{sr}^2T_3I_{max}+\frac{T_3T4I_{max}}{P_{max}}\right)\right), \end{aligned} \quad (15)$$

where, $T_1 = \exp\left(\frac{\sigma_{sr}^2 I_{max}+I_{max}\gamma_{th}\sigma_{se}^2}{\sigma_{ir}^2\gamma_{th}I_{max}\sigma_{se}^2}\right)\left(\frac{(\sigma_{sr}^2)(\sigma_{ri}^2\gamma_{th})^{-L_R-1}}{(\sigma_{se}^2)^{L_R-1}}\right)\times(\gamma_{th}\sigma_{se}^2+\sigma_{sr}^2)^{L_R}$; $T_2 = \frac{\gamma_{th}-1}{I_{max}\gamma th\sigma_{se}^2}$ $T_3 = \frac{\sigma_{sr}^2+\gamma_{th}\sigma_{se}^2}{\sigma_{ir}^2\sigma_{sr}^2\gamma_{th}I_{max}\sigma_{se}^2}$; $T_4 = \sigma_{ir}^2(\gamma_{th}-1)$; $a_1 = \frac{1}{\sigma_{sp}^2}-T_2$; $b_1 = T_3T_4$; and $c_1 = T_3T_4\frac{I_{max}}{P_{max}} + T_3\sigma_{sr}^2 I_{max}$. $\Gamma(.,.)$ is the upper incomplete Gamma function defined in [24] Eq. (8.2.2). $E_i(.)$ is the exponential integral function defined in [24] Eq. (6.2.25).

Proof: See Appendix A.

Similar to the definition of P_1, the P_2 term is defined as

$$P_2 = \int_0^{\infty} F_G\left(\frac{(\gamma_{th}-1)}{P_{max}} + \gamma_{th}y\right) f_{h_{se}}(y) dy. \quad (16)$$

The integral in Eq. (16) can be solved by substituting $F_G(\mathrm{g})$ and $f_{h_{se}}(y)$ that denotes the PDF of the Rayleigh channel gain (i.e., $f_{h_{se}}(y) = \left(\frac{1}{\sigma_{se}^2}\right)\exp\left(-\frac{y}{\sigma_{se}^2}\right)$). Please see Appendix A for the steps to obtain $F_G(\mathrm{g})$.

P_2 can be obtained as follows:

$$\begin{aligned} P_2 &= 1 - \exp\left(\frac{\sigma_{ir}^2(\gamma_{th}-1)+P_{max}(\sigma_{sr}^2+\gamma_{th}\sigma_{se}^2)}{\sigma_{ir}^2\gamma_{th}\sigma_{se}^2P_{max}}\right) \\ &\times\left(\frac{\sigma_{sr}^2\sigma_{ri}^{2\,L_R-1}}{\sigma_{se}^2}\right)\left(\frac{\gamma_{th}\sigma_{se}^2+\sigma_{sr}^2}{\sigma_{se}^2}\right)^{L_R} \\ &\times\Gamma\left(-L_R,\left(\frac{(\sigma_{sr}^2+\gamma_{th}\sigma_{se}^2)(\sigma_{ir}^2(\gamma_{th}-1)+\sigma_{sr}^2P_{max})}{\sigma_{ir}^2\gamma_{th}\sigma_{sr}^2\sigma_{se}^2P_{max}}\right)\right) \end{aligned}. \quad (17)$$

The term is equal to the CDF of $|h_{sp}|^2$ and can be easily calculated as follows:

$$P_3 = \int_{\frac{I_{max}}{P_{max}}}^{\infty} f_{h_{sp}}(w) dw = 1 - \exp\left(-\frac{I_{max}}{\sigma_{sp}^2 P_{max}}\right). \quad (18)$$

The CDF of the first hop $F_{y_{sr}}(y_{th})$ can be obtained using $P1$, $P2$, and $P3$:

$$F_{\gamma_{sr}}(\gamma_{th}) = P_1 + (P_2 \times P_3) \tag{19}$$

The similar derivation steps can be repeated to obtain the second-hop CDF of $F_{y_{rd}}(y_{th})$ by replacing σ_{sr}^2, σ_{sp}^2, σ_{pr}^2, σ_{ir}^2 , and L_R with σ_{rd}^2, σ_{rp}^2, σ_{pd}^2, σ_{id}^2 , and L_D, respectively. Lastly, the SOP of a dual-hop UCRN can be obtained by substituting what was given in Eq. (12).

Strictly Positive Secrecy Capacity

The SPSC is defined as the probability of the instantaneous secrecy achievable rate greater than zero. When the threshold value was set to zero, Eq. (11) is rewritten for the SPSC as follows:

$$SPSC_{e2e} = \Pr\left(\min\left(\underbrace{log_2\left(\frac{1+\gamma_{sr}^{eq}}{1+\gamma_{se}^{eq}}\right)}_{C_{sr}}, \underbrace{log_2\left(\frac{1+\gamma_{rd}^{eq}}{1+\gamma_{re}^{eq}}\right)}_{C_{rd}}\right) > 0\right), \tag{20}$$

$$= \left[1 - F_{\gamma_{spscSR}}(\gamma)\right]\left[1 - F_{\gamma_{spscRD}}(\gamma)\right], \tag{21}$$

where, $F_{y_{spscSR}}(y_{th})$ and $F_{y_{spscRD}}(y_{th})$ denote the CDF of the first and second hops, respectively.

Proposition 2: The SPSC of the first hop $F_{y_{spscSR}}(y_{th})$) can be obtained as

$$F_{\gamma_{spscSR}}(\gamma) = 1 - \frac{\exp\left(\frac{\sigma_{sr}^2+\sigma_{se}^2}{\sigma_{ir}^2\sigma_{se}^2}\right)}{\sigma_{se}^2}\left(\frac{1}{\sigma_{sr}^2}+\frac{1}{\sigma_{se}^2}\right)^{L_R} \times \left(\frac{\sigma_{ir}^2}{\sigma_{sr}^2}\right)^{-1-L_R} \Gamma\left(-L_R, \frac{\sigma_{sr}^2+\sigma_{se}^2}{\sigma_{ir}^2\sigma_{se}^2}\right). \tag{22}$$

Proof: See Appendix B

Using derivation steps similar to $F_{y_{spscSR}}(y_{th})$, $F_{y_{spscRD}}(y_{th})$, can be obtained by replacing the parameters.

Simulation Results

This section presents the simulation results of the SOP and the SPSC together with their analytical results. While the analytical derivation was done with MATHEMATICA, all simulations were performed using Monte Carlo with 10^6 iterations on MATLAB. The simulation results were validated with the analytical results.

The following network parameter values were used in all figures: $P_{max} = 1$ dB, $I_{max} = 2$ dB, and $y_{th} = 1$ dB. Lastly, the AWGN variances at all nodes were set to 1. The average SINR of the main link is defined as the ratio between the variance of the SU nodes and the variance of the eavesdropping channel. The eavesdropping channel variances were set as. The analytical results in Figures 2–4 and 5–6 were obtained from Eqs. (19) and (21), respectively. The CCI and PN interference powers were assumed as dB.

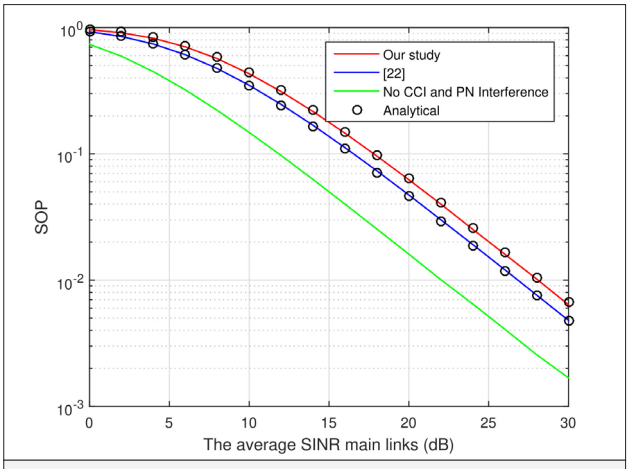

Figure 2. SOP vs. the average SINR of the main link by taking into account only CCI [22], both CCI and primary network interference effect, and no interference effect.

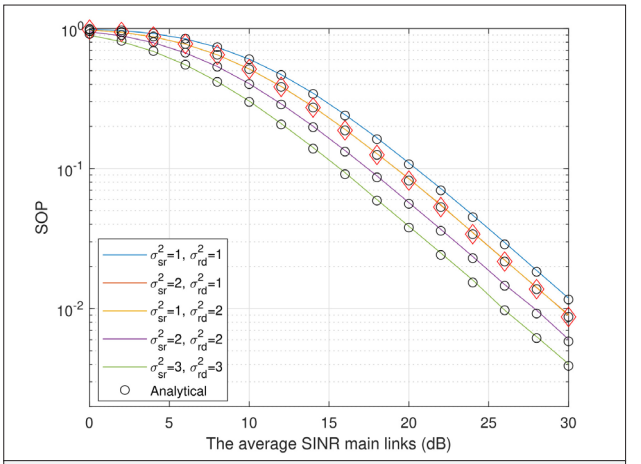

Figure 3. Effects of the average SINR of the main link for various a σ_{sr}^2 and σ_{rd}^2.

Figure 2 depicts the SOP variation versus the average SINR of the main link with the effects of only the CCI in [22] and both the CCI and the PN interference. The SOP in this figure is also shown for the case in which there is neither CCI nor primary source interference. In the simulations, the channel variances were set as $\sigma_{sr}^2 = \sigma_{rd}^2 = \sigma_{sp}^2 = \sigma_{rp}^2 = 2$. Furthermore, the interference channel variances were selected as $\sigma_{pr}^2 = \sigma_{pd}^2 = \sigma_{ir}^2 = \sigma_{id}^2 = 1$. The number of the CCI sources at nodes R and D was assumed to be $L_R = 2$ and $L_D = 2$, respectively. These system parameters were taken from [11] and [22]. Although the SN performance was affected by the existence of both the CCI and the PN interference, only the CCI effect was investigated in [22]. The PN and the SN can simultaneously transmit their data in the UCRN; thus, the SN was exposed to the PN interference. The PN inter-

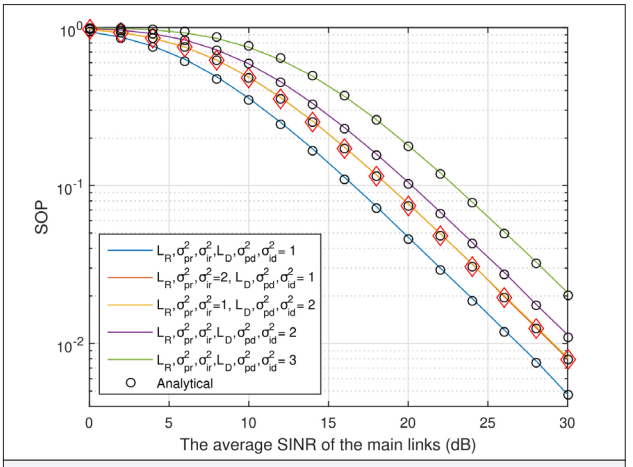

Figure 4. SOP vs. the average SINR of the main link with different number of CCI sources (L_R and L_D) and PN interference channel variance.

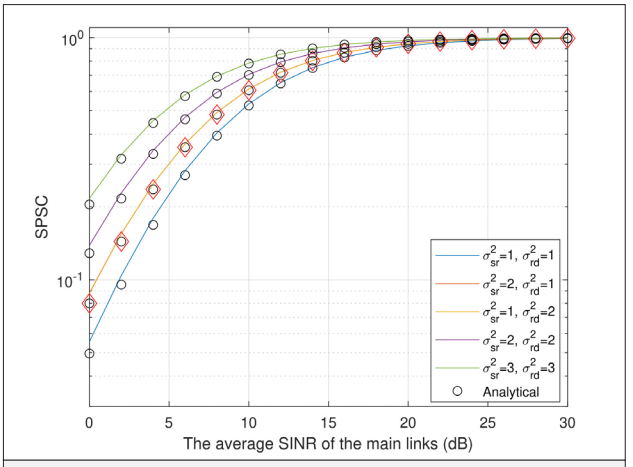

Figure 5. SPSC vs. the average SINR of the main link for various σ_{sr}^2 and σ_{rd}^2 values.

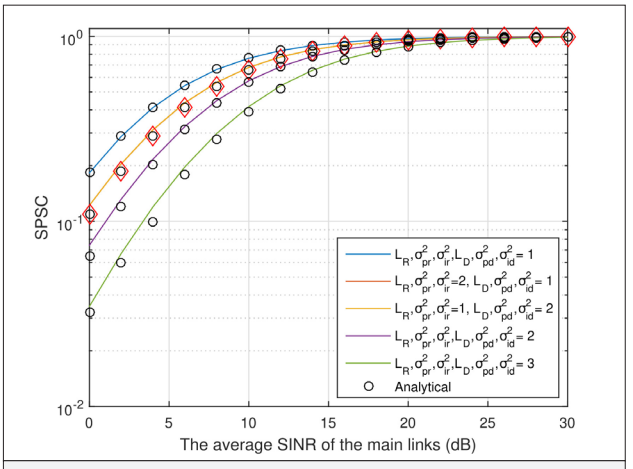

Figure 6. SPSC vs. the average SINR of the main link with different number of CCI sources (L_R and L_D) and PN interference channel variance.

ference to the SN should be considered for achieving a more realistic analysis. The SOP value was at when only the CCI existed. The SOP value was at .

Figure 3 shows the effects of the average main link SINR for various channel variances of $S-R$ and $R-D$. The interference channel variances were selected as $\sigma_{pr}^2 = \sigma_{pd}^2 = \sigma_{ir}^2 = \sigma_{id}^2 = 1$. Furthermore, the numbers of the CCI sources at R and D were selected as $L_R = 2$ and $L_D = 2$, respectively. The system performance evidently improved as the average SINR of the main link increase. The SOP decreased as the quality of the S–R and R–D links was improved, indicating that the high variance improved the SOP. For example, in an SINR of dB, the SOP value for $\sigma_{sr}^2 = \sigma_{rd}^2 = 3$ was better than that for $\sigma_{sr}^2 = \sigma_{rd}^2 = 2$. Moreover, the same SOP curve was obtained for the case of $\sigma_{sr}^2 = 1$, $\sigma_{rd}^2 = 2$ and $\sigma_{sr}^2 = 1$, $\sigma_{rd}^2 = 2$ due to the DF strategy used in the SN.

In Figure 4, the impact of the PN interference channel variance and the number of the CCI sources on the system performance were investigated by linearly increasing them. The main link variances were set to . In this analysis, the PN interference channel variances at the R and D nodes were selected as $\sigma_{ir}^2 = \sigma_{pr}^2 = L_R$ and $\sigma_{id}^2 = \sigma_{pd}^2 = L_D$, respectively. A degradation can be observed as the number of CCI sources and PN interference channel variance increased.

Figure 5 presents the SPSC variation versus the average SINR of the main link for various σ_{sr}^2 and σ_{rd}^2 values. The SPSC value approached 1 for all σ_{sr}^2 and σ_{rd}^2 values as the SINR of the main link increased. The SPSC performed better when the main link channel powers were $\sigma_{sr}^2 = 3$ and $\sigma_{rd}^2 = 3$. The separation between the curves decreased after $SINR = 0$ dB.

Figure 6 depicts the impact of the PN interference and the CCI on the SPSC. In this analysis, the PN interference channel variances at nodes R and D were selected as $\sigma_{ir}^2 = \sigma_{pr}^2 = L_R$ and $\sigma_{id}^2 = \sigma_{pd}^2 = L_D$, respectively. Moreover, the variances of the S–R and R–D links were selected as $\sigma_{sr}^2 = \sigma_{rd}^2 = 2$. As expected, the SPSC value decreased as the number of CCI sources and PN interference channel variance increased. The SPSC value was 0.4502 when the number of CCI sources was L_R and $L_D = 2$ at $SINR = 10$ dB and 0.2996 at $SINR = 10$ dB when L_R and $L_D = 3$.

Conclusions

This study investigated the SOP of the dual-hop DF UCRN system in the presence of the CCI and the PN interference over slow Rayleigh fading channels. The analytical SOP and SPSC results were derived along with the simulation results. The analytical results evidently matched well with the Monte Carlo simulation results.

The CCI from the undesired sources and the PN interference in the SN degraded the SOP and SPSC performances. This study showed the importance of considering the impact of the PN interference. We also observed that I_{max}, P_{max}, and $|h_{sp}|^2$ do not affect the SPSC, as can be seen from Eq. (46).

Appendix A

Proof of Proposition 1

The CDF of F_X can be written as

$$F_X(z) = Pr(X < z), \tag{23}$$

$$= Pr\left(\frac{|h_{sr}|^2}{1+\sum_{j=1}^{L_R}\left|h_{ir_j}\right|^2+\left|h_{pr}\right|^2} < \frac{(\gamma_{th}-1)}{I_{max}}z + \gamma_{th} + |h_{se}|^2\right), \tag{24}$$

$$= \int_0^\infty F_G\left(\frac{\gamma_{th}-1}{I_{max}}z + \gamma_{th}y\right) f_{h_{se}}(y), \tag{25}$$

where, $G = \left(\frac{|h_{sr}|^2}{1+\sum_{j=1}^{L_R}\left|h_{ir_j}\right|^2+\left|h_{pr}\right|^2}\right)$ and $f_{h_{se}}(y)$ denote the PDF of the Rayleigh channel gain (i.e., $f_{h_{se}}(y) = \left(\frac{1}{\sigma_{se}^2}\right)\exp\left(-\frac{y}{\sigma_{se}^2}\right)$).

First, the CDF of F_G should be calculated to obtain F_X. G can be expressed as $G = \left(\frac{C}{1+A+B}\right)$, where A, B, and C are random variables (RVs) for $\sum_{j=1}^{L_R}\left|h_{ir_j}\right|^2+\left|h_{pr}\right|^2$, $\left|h_{pr}\right|^2$, and $|h_{sr}|^2$, respectively. The PDF of A, B, and C can be written as follows:

$$f_{A_1}(a_1) = \left(\frac{{a_1}^{L_R-1}}{{\sigma_{ir}^2}^{L_R}\Gamma(L_R)}\right)\exp\left(-\frac{a_1}{\sigma_{ir}^2}\right), \tag{26}$$

$$f_{B_1}(b_1) = \left(\frac{1}{\sigma_{pr}^2}\right)\exp\left(-\frac{b_1}{\sigma_{pr}^2}\right), \tag{27}$$

$$f_{C_1}(c_1) = \left(\frac{1}{\sigma_{sr}^2}\right)\exp\left(-\frac{c_1}{\sigma_{sr}^2}\right). \tag{28}$$

The first step of obtaining $F_G(g)$ is finding the PDF of the sum of the two RVs $(U = A + B)$. This can be done by using the following formula:

$$f_U(u) = \int_0^u f_{A_1}(a_1) f_{B_1}(u-a_1) da_1. \tag{29}$$

$f_u(u)$ can be obtained as follows:

$$f_U(u) = \frac{\exp\left(-\frac{u}{\sigma_{pr}^2}\right)\left(\frac{\sigma_{pr}^2}{\sigma_{pr}^2-\sigma_{ir}^2}\right)^{L_R}}{\sigma_{pr}^2\Gamma(L_R)}\gamma\left(L_R, \frac{(\sigma_{pr}^2-\sigma_{ir}^2)u}{\sigma_{pr}^2\sigma_{ir}^2}\right), \tag{30}$$

where $\gamma(.,.)$ is the upper incomplete Gamma function defined in [24] Eq. (8.2.1). In the next step, the CDF of $G = \frac{C}{1+U}$ can be obtained using the following formula, which is the CDF of the RV division.

$$F_G(g) = \int_0^\infty F_{C_1}(g(u+1) f_U(u) du. \tag{31}$$

F_{c1} can be directly obtained from Eq. (28), and $F_G(g)$ can be obtained as follows:

$$F_G(g) = 1 - \exp\left(-\frac{g}{\sigma_{sr}^2}\right)\left(\frac{\sigma_{sr}^2}{\sigma_{sr}^2+g\sigma_{pr}^2}\right)\left(\frac{\sigma_{sr}^2}{\sigma_{sr}^2+g\sigma_{ir}^2}\right)^{L_R}. \tag{32}$$

The integral in Eq. (25) can be solved by substituting $F_G(g)$ and $f_{h_{se}}(y)$. $F_X(z)$ can then be written as follows:

$$F_X(z) = 1 - T_1\exp(T_2 z)\Gamma(-L_R, T_3(T_4 z + \sigma_{sr}^2 I_{max})). \tag{33}$$

The Gamma function should be simplified according to [55] Eq. (8.4.15) to solve the integral in Eq. (14).

$$\begin{aligned}&\Gamma(1-L_R, T_3T_4z + T_3{\sigma_{sr}}^2 I_{max})\\ &= \underbrace{-\frac{(-1)^{L_R}}{L_R!}Ei\left((T_3T_4z + T_3{\sigma_{sr}}^2 I_{max})\right)}_{B_1}\\ &\underbrace{-\frac{(-1)^{L_R}}{L_R!}\sum_{n=0}^{L_R-1}\frac{exp(T_3T_4z + T_3{\sigma_{sr}}^2 I_{max})(-1)^n n!}{(T_3T_4z + T_3{\sigma_{sr}}^2 I_{max})^{n+1}}}_{B_2}.\end{aligned} \tag{34}$$

$$= -B_1 - B_2. \tag{35}$$

P_1 can be rewritten as follows after simplification:

$$\begin{aligned}P_1 &= \underbrace{\int_{\frac{I_{max}}{P_{max}}}^\infty \frac{1}{\sigma_{sp}^2}exp(-\frac{1}{\sigma_{sp}^2}z)\,dz}_{I_1}\\ &\underbrace{+\int_{\frac{I_{max}}{P_{max}}}^\infty T_1B_1\frac{1}{\sigma_{sp}^2}exp((T_2-\frac{1}{\sigma_{sp}^2})z)\,dz}_{I_2}\\ &\underbrace{+\int_{\frac{I_{max}}{P_{max}}}^\infty T_1B_2\frac{1}{\sigma_{sp}^2}exp((T_2-\frac{1}{\sigma_{sp}^2})z)\,dz}_{I_3}.\end{aligned} \tag{36}$$

$$I_1 = exp(-\frac{I_{max}}{\sigma_{sp}^2P_{max}}) \tag{37}$$

I_1 can be directly derived as follows:

$$I_1 = exp(-\frac{I_{max}}{\sigma_{sp}^2P_{max}}) \tag{38}$$

I_2 can be rewritten as follows:

$$\begin{aligned}I_2 &= \frac{T_1(-1)^{L_R}}{L_R!\,\sigma_{sp}^2}exp(-(\frac{1}{\sigma_{sp}^2}-T_2)\frac{I_{max}}{P_{max}})\\ &\times\underbrace{\int_0^\infty exp(-(\frac{1}{\sigma_{sp}^2}-T_2)w)}_{P}\\ &\times\underbrace{Ei(-T_3T_4w-(T_3T_4P_{max}+T_3{\sigma_{sr}}^2I_{max}))dw}_{P}.\end{aligned} \tag{39}$$

can be represented in integral form as $P = \int_0^\infty Ei(-bx-c)\,exp(-ax)\,dx$. P can be obtained by using the following formula [22]:

$$\int_0^{\infty} Ei(-bx-c)\,exp(-ax)\,dx = \frac{1}{b}exp\left(\frac{ac}{b}\right) \times \int_c^{\infty} Ei(-t)\,exp\left(\frac{-a}{b}\right) \quad (40)$$

According to (40), I_2 can be obtained as follows:

$$I_2 = \left(\frac{T_1(-1)^{L_R}}{L_R!\,\sigma_{sp}^2} exp\left(-\left(\frac{1}{\sigma_{sp}^2}-T_2\right)\frac{I_{max}}{P_{max}}\right)\right)\left(\frac{1}{a_1\sigma_{sr}^2 L_R!}\right) \times \left(Ei(-c_1)-exp\left(\frac{a_1c_1}{b_1}\right)Ei\left(-c_1-\frac{a_1c_1}{b_1}\right)\right) \quad (41)$$

where, $a_1 = \frac{1}{\sigma_{sp}^2} - T_2$, $b_1 = T_3T_4$, $c_1 = T_3T_4\frac{I_{max}}{P_{max}} + T_3\sigma_{sr}^2 I_{max}$.

In the next step, I_3 can be rewritten as follows:

$$I_3 = \underbrace{\sum_{n=0}^{L_R-1}\frac{T_1(-1)^{L_R}}{\sigma_{sp}^2 L_R!}(-1)^n n!}_{G_1} \times \int_{\frac{I_{max}}{P_{max}}}^{\infty} exp\left((T_2-\frac{1}{\sigma_{sp}^2})z\right)\frac{exp(T_3T_4z+T_3{\sigma_{sr}}^2 I_{max})}{(T_3T_4z+T_3{\sigma_{sr}}^2 I_{max})^{n+1}}dz. \quad (42)$$

Now, let $s = T_3T_4z + T_3\,\sigma_{sr}^2 I_{max}$. The following expression is obtained:

$$I_3 = \underbrace{G_1\,exp\left(\left(\frac{1}{\sigma_{sp}^2}-T_2\right)\frac{{\sigma_{sr}}^2 I_{max}}{T_4}\right)\frac{1}{T_3T_4}}_{G_2} \times \int_{T_3T_4\frac{I_{max}}{P_{max}}+T_3{\sigma_{sr}}^2 I_{max}}^{\infty}\frac{exp\left(-\left(\frac{1}{\sigma_{sp}^2T_3T_4}-\frac{T_2}{T_3T_4}+1\right)s\right)}{s^{n+1}}ds. \quad (43)$$

Next, the variable in Eq. (43) is changed to $t = \left(\frac{1}{\sigma_{sp}^2T_3T_4}-\frac{T_2}{T_3T_4}+1\right)s$. I_3 can be rewritten as follows after this substitution and through mathematical manipulation:

$$I_3 = \underbrace{G_2\left(\frac{1}{{\sigma_{sr}}^2T_3T_4}-\frac{T_2}{T_3T_4}+1\right)^n}_{G_3} \times \int_{\left(\frac{1}{\sigma_{sp}^2T_3T_4}-\frac{T_2}{T_3T_4}+1\right)\left(T_3T_4\frac{I_{max}}{P_{max}}+T_3\beta_1 I_{max}\right)}^{\infty}\frac{exp(-t)}{t^{n+1}}dt. \quad (44)$$

According to [25] Eq. (8.350.2), can be obtained as follows:

$$I_3 = \sum_{n=0}^{L_R-1}\frac{T_1(-1)^{L_R}}{T_3T_4\sigma_{sp}^2L_R}(-1)^n n! \times \left(\frac{1}{T_3T_4\sigma_{sp}^2}-\frac{T_2}{T_3T_4}+1\right)^n \times exp\left(\frac{\left(\frac{1}{\sigma_{sp}^2}-T_2\right)\sigma_{sr}^2 I_{max}}{T_4}\right) \times \Gamma\left(-n,\left(\frac{1}{T_3T_4\sigma_{sp}^2}-\frac{T_2}{T_3T_4}+1\right)\left(\sigma_{sr}^2T_3I_{max}+\frac{T_3T4I_{max}}{P_{max}}\right)\right). \quad (45)$$

Appendix B

Proof of Proposition 2

The SPSC of the first hop ($F_{y_{spsc_{SR}}}(y)$) can be defined as follows using the definition in Eq. (20):

$$F_{\gamma_{spsc_{SR}}}(\gamma) = Pr(C_{SR}>0) = \Pr\left(\gamma_{sr}^{eq} > \gamma_{se}^{eq}\right) = \Pr\left(\frac{|h_{sr}|^2}{1+\sum_{j=1}^{L_R}\left|h_{ir_j}\right|^2+\left|h_{pr}\right|^2} > |h_{se}|^2\right). \quad (46)$$

Eq. (46) can be expressed in an integral form as follows:

$$F_{\gamma_{spsc_{SR}}}(\gamma) = \int_0^{\infty} F_G(y)\,f_{h_{se}}(y)dy. \quad (47)$$

$F_{y_{spsc_{SR}}}$ is obtained as follows after solving the integral:

$$F_{\gamma_{spsc_{SR}}}(\gamma) = 1 - \frac{\exp\left(\frac{\sigma_{sr}^2+\sigma_{se}^2}{\sigma_{ir}^2\sigma_{se}^2}\right)}{\sigma_{se}^2} \times \left(\frac{1}{\sigma_{sr}^2}+\frac{1}{\sigma_{se}^2}\right)^{L_R}\left(\frac{\sigma_{ir}^2}{\sigma_{sr}^2}\right)^{-1-L_R}\Gamma\left(-L_R,\frac{\sigma_{sr}^2+\sigma_{se}^2}{\sigma_{ir}^2\sigma_{se}^2}\right). \quad (48)$$

Peer-review: Externally peer-reviewed.

Conflict of Interest: The authors have no conflicts of interest to declare.

Financial Disclosure: The authors declared that the study has received no financial support.

References

1. H. Holma, A. Toskala, T. Nakamura, "5G technology: 3GPP new radio", Wiley, USA, 2020. [Crossref]
2. S. Haykin, "Cognitive radio: brain-empowered wireless communications", IEEE Journal on Selected Areas in Communications, vol. 23, no. 2, pp. 201-220, Feb. 2005. [Crossref]
3. A. Goldsmith, S. A. Jafar, I. Maric, S. Srinivasa, "Breaking spectrum gridlock with cognitive radios: an information theoretic perspective", Proceedings of the IEEE, vol. 97, no. 5, pp. 894-914, May, 2009. [Crossref]
4. J. Lee, H. Wang, J. G. Andrews, D. Hong, "Outage probability of cognitive relay networks with ınterference constraints", IEEE Trans. Wirel. Commun., vol. 10, no. 2, pp. 390-395, Feb. 2011. [Crossref]
5. L. Luo, P. Zhang, G. Zhang, J. Qin, "Outage performance for cognitive relay networks with underlay spectrum sharing", IEEE Commun. Lett., vol. 15, no. 7, pp. 710-712, July, 2011. [Crossref]
6. C. Zhong, T. Ratnarajah, K.-K. Wong, "Outage analysis of decode and forward cognitive dual-hop systems with the interference constraint in Nakagami-m fading channels", IEEE Trans. Veh. Technol., vol. 60, no. 6, pp. 2875-2879, July, 2011. [Crossref]
7. G. Chen, Z. Tian, Y. Gong, J. Chambers, "Decode and forward buffer-aided relay selection in cognitive relay networks", IEEE Trans. Veh. Technol., vol. 63, no. 9, pp. 4723-4728, Nov. 2014. [Crossref]
8. K. Ho-Van, P. C. Sofotasios, G. C. Alexandropoulos, S. Freear, "Bit error rate of underlay decode and forward cognitive networks with

best relay selection", Journal of Communication and Networks, vol. 17, no. 2, pp. 162-171, Apr. 2015. [Crossref]

9. J. A. Hussein, S. S. Ikki, S. Boussakta, C. C. Tsimenidis, "Performance analysis of opportunistic scheduling in dual-hop multiuser underlay cognitive network in the presence of co-channel interference", IEEE Transactions on Vehicular Technology, vol. 65, no. 10, pp. 8163-8176, Oct. 2016. [Crossref]
10. J. A. Hussein, S. S. Ikki, S. Boussakta, C. Tsimenidis, "Performance study of the dual-hop underlay cognitive network in the presence of co-channel interference", 2015 IEEE 81st Vehicular Technology Conference (VTC Spring), pp. 1-5, Glasgow, 2015. [Crossref]
11. J. A. Hussein, S. Boussakta, S. S. Ikki, "Performance study of a UCRN over nakagami- m fading channels in the presence of cci", IEEE Transactions on Cognitive Communications and Networking, vol. 3, no. 4, pp. 752-765, Dec. 2017. [Crossref]
12. J. A. Hussein, S. S. Ikki, S. Boussakta, C. C. Tsimenidis, J. Chambers, "Performance Analysis of a Multi-Hop UCRN With Co-Channel Interference", IEEE Transactions on Communications, vol. 64, no. 10, pp. 4346-4364, Oct. 2016. [Crossref]
13. A. D. Wyner, "The wire-tap channel", The Bell System Technical Journal, vol. 54, no. 8, pp. 1355-1387, Oct. 1975. [Crossref]
14. I. Csiszar, J. Korner, "Broadcast channels with confidential messages", IEEE Transactions on Information Theory, vol. 24, no. 3, pp. 339-348, May, 1978. [Crossref]
15. Z. Shu, Y. Qian, S. Ci, "On physical layer security for cognitive radio networks", IEEE Network, vol. 27, no. 3, pp. 28-33, June, 2013. [Crossref]
16. Y. Zou, J. Zhu, L. Yang, Y. Liang, Y. Yao, "Securing physical layer communications for cognitive radio networks", IEEE Communications Magazine, vol. 53, no. 9, pp. 48-54, Sept. 2015. [Crossref]
17. Y. Pei, Y. Liang, L. Zhang, K. C. Teh and K. H. Li, "Secure communication over MISO cognitive radio channels", IEEE Transactions on Wireless Communications, vol. 9, no. 4, pp. 1494-1502, Apr. 2010. [Crossref]
18. M. Elkashlan, L. Wang, T. Q. Duong, G. K. Karagiannidis, A. Nallanathan, "On the Security of Cognitive Radio Networks," IEEE Transactions on Vehicular Technology, vol. 64, no. 8, pp. 3790-3795, Aug. 2015. [Crossref]
19. H. Lei, H. Zhang, I. S. Ansari, Z. Ren, G. Pan, K. A. Qarage, M. S. Alauini, "On secrecy outage of relay selection in underlay cognitive radio networks over Nakagami- m fading channels", IEEE Transactions on Cognitive Communications and Networking, vol. 3, no. 4, pp. 614-627, Dec. 2017. [Crossref]
20. R. Zhao, Y. Yuan, L. Fan, Y. C. He, "Secrecy performance analysis of cognitive decode and forward relay networks in Nakagami-m fading channels", IEEE Trans. Commun., vol. 65, no. 2, pp. 549-563, Feb. 2017 [Crossref]
21. H. Lei, C. Gao, Y. Guo and G. Pan, "On physical layer security over generalized Gamma fading channels", IEEE Commun. Lett., vol. 19, no. 7, pp. 1257-1260, July, 2015. [Crossref]
22. Q. Yang, J. Ding, A. Hu, "Secrecy outage performance analysis of DF cognitive relay network with co-channel interference", Wireless Personal Communications, vol. 107, no. 1, pp. 549-564, 2019. [Crossref]
23. D. Tse, P. Viswanath, "Fundamentals of wireless communication", Cambridge: Cambridge University Press, 2005. [Crossref]
24. F. W. Olver, D. W. Lozier, R. F. Boisvert, C.W Clark, "NIST handbook of mathematical functions", 1st ed. Cambridge: Cambridge University Press, 2010.
25. I. S. Gradshteyn, M. Ryzhikl, "Table of integrals, series and products", 7th ed. New York: Academic Press, 2007.

Emre Bayat received the B.S degree in Electronics and Communications Engineering from Kocaeli University, Kocaeli 2015 and started M.S degree in Electronics and Communications Engineering from Kocaeli University, Kocaeli 2017. He is currently working as a Radio Network Consultant in P.I Works Inc. since 2015.

Sultan Aldırmaz Çolak received the B.S degree in Electronics and Communications Engineering from Kocaeli University, Kocaeli 2004 and the M.S. and PhD degrees in Yildiz Technical University (YTU), Istanbul in 2006 and 2012, respectively. She was a visiting research scholar in the Department of Electrical and Computer Engineering of University of South Florida for the spring and summer of 2009. She is currently an Assistant Professor in the Electronics and Communications Engineering Department of Kocaeli University, Kocaeli, Turkey. Her primary research interests include MIMO systems, index modulation, OFDM, and visible light communications.